JACS
JOURNAL OF THE AMERICAN CHEMICAL SOCIETY
Communication
pubs.acs.org/JACS

Core–Shell Palladium Nanoparticle@Metal–Organic Frameworks as Multifunctional Catalysts for Cascade Reactions

Meiting Zhao,[†] Ke Deng,[†] Liangcan He,[†] Yong Liu,[†] Guodong Li,*[,†] Huijun Zhao,[‡] and Zhiyong Tang*[,†]

[†]Laboratory for Nanomaterials, National Center for Nanoscience and Technology, Beijing, 100190, P. R. China
[‡]Centre for Clean Environment and Energy, Gold Cost Campus, Griffith University, Queensland, 4222, Australia

Supporting Information

ABSTRACT: Uniform core–shell Pd@IRMOF-3 nanostructures, where single Pd nanoparticle core is surrounded by amino-functionalized IRMOF-3 shell, are prepared by a facile mixed solvothermal method. When used as multifunctional catalysts, the Pd@IRMOF-3 nanocomposites exhibit high activity, enhanced selectivity, and excellent stability in the cascade reaction. Both experimental evidence and theoretical calculations reveal that the high catalytic performance of Pd@IRMOF-3 nanocomposites originates from their unique core–shell structures.

Metal–organic frameworks (MOFs), which are synthesized by self-assembly of metal ions or clusters with polytopic organic linkers,[1] have been attracting much attention in heterogeneous catalysis due to their intriguing features including extraordinarily large surface area, well-defined pore structure, easy tailorable chemistry, and high acid–base catalytic activities.[2] Unfortunately, previous works are mainly focused on investigation of single-step reaction using MOF-based catalysts,[2,3] and the multistep cascade reactions are rarely reported, though such reactions are extremely important for sustainable synthesis with lower cost, fewer chemicals, and less energy consumptions.[4]

To implement the high-efficient cascade reactions, a plausible way is to integrate two components of different catalytic functions like MOFs and noble metal nanoparticles (NPs) into a single nanostructure.[5] Among various composites of MOFs and noble metal NPs developed, the obtained structures are generally characteristic of noble metal NPs either onto the outside of MOFs[5a,b] or into the pores of MOFs.[5c−f] In the former case, the noble metal NPs attached on the MOF surfaces have high surface energy and tend to migrate and aggregate into larger particles, leading to loss of the catalytic activity during continuous reactions. While in the latter case, the size, shape and spatial distribution of noble metal NPs embedded in the MOFs are hardly controlled, and furthermore incorporation of NPs inside the MOF pores would block the mass transport of both reactants and products, giving rise to low and unreliable catalytic activity.[6] Therefore, it is highly desirable to develop novel ways to construct the well-defined noble metal NP/MOF nanostructures, which not only make the noble metal NPs well dispersed and against migration and aggregation but also guarantee the MOF pores accessible for both reactants and products.[7]

In this work, we propose that the uniform core–shell nanostructures composed of the Pd NP core[8] and the amino-functionalized isoreticular MOF-3 (IRMOF-3) shell[9] could be used as the multifunctional catalysts for the cascade reactions (Scheme 1). The model cascade reaction is designed as

Scheme 1. (a) Synthetic Route for the Core–Shell Pd@IRMOF-3 Hybrids via the Mixed Solvothermal Method and (b) Model Cascade Reactions Involving Knoevenagel Condensation of A and Malononitrile via the IRMOF-3 Shell And Subsequent Selective Hydrogenation of Intermediate Product B to C via the Pd NP Cores

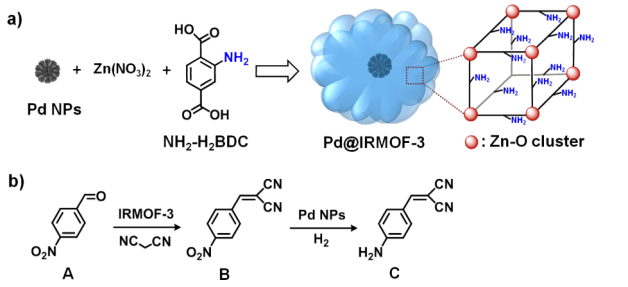

Knoevenagel condensation of 4-nitrobenzaldehyde (**A**) and malononitrile[10] into 2-(4-nitrobenzylidene)malononitrile (**B**) via the alkaline IRMOF-3 shells, followed by selective hydrogenation of $-NO_2$ group of the intermediate products **B** by the Pd NP cores (Scheme 1b). The reason to study this cascade reaction is that the target product, 2-(4-aminobenzylidene)-malononitrile (**C**), has been known as a key intermediate in the synthesis of dyes and antihypertensive drugs.[11] Impressively, such a novel type of core–shell Pd@IRMOF-3 catalyst exhibits superior catalytic performance compared with the supported Pd/IRMOF-3 hybrids.

In brief, synthesis of core–shell Pd@IRMOF-3 nanostructures involves the dissolution of precursors $Zn(NO_3)_2$ and 2-amino terephthalic acid (NH_2-H_2BDC) in the mixed solvent containing polyvinylpyrrolidone (PVP), *N*,*N*-dimethylformamide (DMF), and ethanol, followed by addition of presynthesized Pd NPs and subsequent solvothermal treatment. The morphology and structure of as-prepared Pd@IRMOF-3 nanocomposites are first investigated by different characterization techniques, and several important features can be distinguished: (1) The products are of the monodisperse spherical shape (Figure 1a) with the typical core–shell structure (Figure 1b,c), for which a Pd NP core of ~35 nm in diameter is coated with a uniform

Received: November 11, 2013
Published: January 17, 2014

   dx.doi.org/10.1021/ja411468e | J. Am. Chem. Soc. 2014, 136, 1738–1741

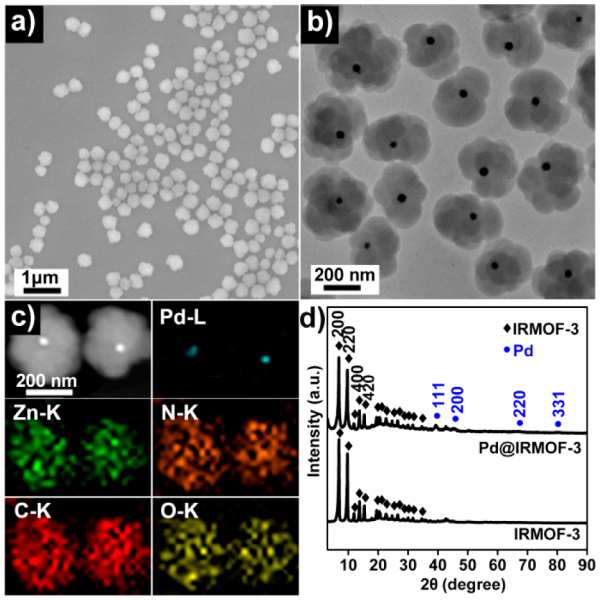

Figure 1. (a) SEM image of the core−shell Pd@IRMOF-3 nanocomposites. (b) TEM image of the nanocomposites. (c) HAADF-STEM image and corresponding EDX elemental mapping image of the nanocomposites. (d) XRD patterns of Pd@IRMOF-3 and pure IRMOF-3.

IRMOF-3 shell of ~145 nm in thickness (Figure S1). (2) Crystal structure analysis from powder X-ray diffraction (XRD) pattern reveals two sets of peaks, which are ascribed to face-centered-cubic phase of Pd and cubic phase of IRMOF-3 (Figure 1d),[8,9] respectively. It should be noted that the high-resolution transmission electron microscopy (HRTEM) images (Figure S2) of the Pd core and IRMOF-3 shell cannot be clearly recognized, likely due to the fact that the Pd NP core is encapsulated by the thick shell and IRMOF-3 is unstable under illumination of high energy electron beam.[12] (3) Fourier transform infrared (FTIR) spectrum (Figure S3) further shows that the characteristic −OH stretching frequency in the carboxylic acid group of the NH_2-H_2BDC linker centered at 2970 cm^{-1} disappears after formation of the Pd@IRMOF-3 nanocomposites, suggesting occurrence of the coordination interaction between Zn^{2+} ions and carboxylic acid group of NH_2-H_2BDC to form IRMOF-3. In addition, two peaks at around 3450 and 3350 cm^{-1}, attributing to the asymmetric and symmetric stretching absorptions of primary amine group,[10b] can be clearly discerned. This result indicates that the amino groups in the IRMOF-3 products are fully retained. Evidently, using the facile mixed solvothermal method is an effective way to construct the well-defined core−shell Pd@IRMOF-3 nanocomposites.

The detailed formation mechanism of the core−shell Pd@IRMOF-3 nanostructures is elucidated by a series of control experiments including variation of PVP amount, ethanol/DMF ratio, and crystallization time. Figure S4 discloses that PVP not only functionalizes as the stabilizers to make the Pd NPs well dispersed but also provides the affinity to adsorb IRMOF-3 precursors onto the Pd NP surfaces via coordination interaction between the pyrrolidone rings (C═O) and Zn^{2+} ions as well as hydrophobic interaction between the apolar groups of PVP and the NH_2-H_2BDC organic linkers.[6b] The mixed solvent is found to be another key to generate core−shell Pd@IRMOF-3 nanostructures. As shown in Figures S5 and S6, in pure ethanol solution there is no IRMOF-3 to be formed, while free IRMOF-3 submicrospheres are produced in pure DMF solution. As comparison, when the mixed solvent of ethanol and DMF is used, the nanocomposites of the distinct core−shell structures are achieved at the volume ratio of ethanol/DMF ranging from 0.5 to 1. This result suggests that the nucleation and growth of IRMOF-3 shells on the surface of Pd NPs could be effectively tuned by the mixed solvent method. Finally, the formation process of the core−shell Pd@IRMOF-3 nanostructures is explored by changing their crystallization time (Figure 2). At

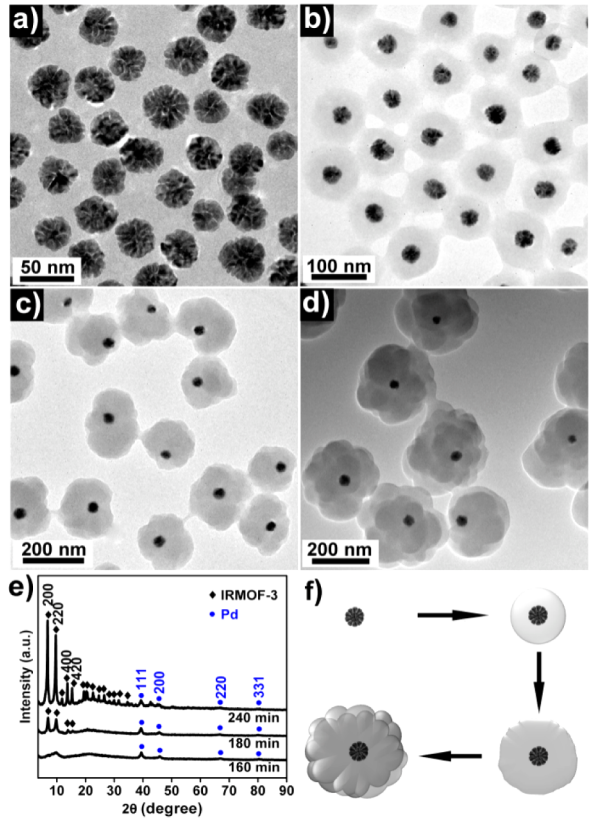

Figure 2. TEM images of the products at various crystallization time: (a) 120, (b) 160, (c) 180, and (d) 240 min and (e) corresponding XRD patterns. (f) Scheme of the formation process of core−shell Pd@IRMOF-3.

reaction time of 120 min, the solution remains clear, and only bare Pd NPs exist (Figure 2a). With the crystallization time is extended to 160, 180, and 240 min (Figure 2b−d), the core−shell nanostructures are obtained, and the shell thicknesses are increased from 30 to 145 nm accompanied with evolution of the shells from amorphous to highly crystalline nature (Figure 2e,f). Such structural transformation is also observed in crystallization of MIL-89(Fe).[13] In addition, no matter how the experimental conditions are changed, there are no obvious changes in the size, shape, and structure of Pd NP cores (Figure 2) in respect to the original Pd NP seeds (Figure S7), providing us the opportunity to control the geometrical parameters of the cores.[14]

The activity of the core−shell Pd@IRMOF-3 nanocomposites as the multifunctional catalysts is evaluated using the cascade reactions (Scheme 1). The contrast samples including bare Pd NPs, pure IRMOF-3, and supported Pd/IRMOF-3 (Figures S7−S9, respectively) are also tested under the same reaction conditions, and the physiochemical properties of different

dx.doi.org/10.1021/ja411468e | J. Am. Chem. Soc. 2014, 136, 1738−1741

samples are tuned to be close with each other (Figures S1, S7–S10, and Table S1). For instance, the content of 35 nm Pd NPs in both the Pd@IRMOF-3 and the Pd/IRMOF-3 is kept the same (~2% by weight), and the average diameters are ranged from 326 nm to 341 nm for different samples. N_2 physisorption measurements reveal that all samples investigated display the typical type I nitrogen sorption isotherms with the steep increase in N_2 uptake at low relative pressure (<0.01). Furthermore, they have the same two types of micropores that are dominantly composed of those of 1.03 nm in diameter along with small percentage of 1.99 nm (Figure S10 and Table S1), suggesting that the introduction of the Pd NP cores does not change the pore size distribution of IRMOF-3 shells. Brunauer–Emmett–Teller (BET) surface area analysis demonstrates that the specific surface areas are 828 $m^2\ g^{-1}$ for Pd@IRMOF-3 and 795 $m^2\ g^{-1}$ for Pd/IRMOF-3, both of which are lower than that of 918 $m^2\ g^{-1}$ for pure IRMOF-3 due to the presence of Pd NPs in the former two samples (Table S1).[6a]

Table 1 summarizes the catalytic performance of different samples for the cascade reactions. As for the Knoevengel

Table 1. Cascade Reactions of Knoevenagel Condensation Coupling with Selective Hydrogenation Reactions Catalyzed by Different Catalysts[a]

samples	$A_{conv.}$ (%)	form.[b] (%)	conv.[c] (%)	sel. (%)		
		B		C	D	E
Pd@IRMOF-3	100	100	100	86	8	6
Pd/IRMOF-3	100	100	100	71	24	5
IRMOF-3	100	100	0	0	0	0
Pd NPs[d]	26	26	–	–	–	–
Pd NPs[e]	–	–	82	68	32	0
blank[f]	26	26	–	–	–	–

[a]Reaction conditions: **A** (0.2 mmol), malononitrile (0.21 mmol), catalyst (10 mg) (see the Supporting Information). [b]**B** is formed via the condensation reaction. [c]Formed **B** is converted via the hydrogenation reaction. [d]For Knoevenagel condensation alone. [e]0.2 mmol **B** is used as the raw material for the hydrogenation reaction. [f]No catalysts are used for the cascade reactions.

condensation of **A** and malononitrile, the carbon–carbon coupling happens to form **B**. Subsequent hydrogenation of the intermediate product **B** is complex, and both $-NO_2$ and C=C groups are likely involved. As a result, except for the target product of **C**, the byproducts like 2-(4-nitrobenzyl)malononitrile (**D**) and 2-(4-aminobenzyl)-malononitrile (**E**) are also generated. When IRMOF-3 is used as the alkaline catalysts for the Knoevengel condensation, **A** is completely converted into **B**; however, no activity for the hydrogenation process is found (Table 1, entry 3). On the contrary, bare Pd NPs demonstrate no activity for the Knoevengel condensation when eliminating the effect of the organic solvents used[15] (Table 1, entries 4 and 6), but they can catalyze the hydrogenation of raw material **B**, ~82% of which is converted to **C** and **D** with the selectivity of 68% and 32% (Table 1, entry 5), respectively. Furthermore, density functional theory (DFT) calculations also indicate that it is more favorable for selective conversion of **B** to **C** rather than **D** over bare Pd NPs based on Gibbs free energy minimization (Figures S11–S13). Different with bare Pd NPs and pure IRMOF-3, both Pd@IRMOF-3 and Pd/IRMOF-3 can catalyze the cascade reactions effectively, however, the compositions of final products are remarkably different, highlighting the importance of the structural design on the nanocatalysts.[16] For core–shell Pd@IRMOF-3 nanocatalysts, the hydrogenation selectivity of **B** to **C**, **D** and **E** is 86%, 8%, and 6% (Table 1, entry 1; Figure S14), respectively; as comparison, the corresponding selectivity is 71%, 24%, and 5% for conventional supported Pd/IRMOF-3 catalysts (Table 1, entry 2). Why the enhanced catalytic selectivity of **B** to **C** can be obtained using the core–shell nanostructures? To understand the reason, the corresponding DFT calculations are preformed. Reactant **A** is a linear molecule (1.03 × 0.72 nm) (Figure S15a), and its selective conversion is substantially affected by the group-selective adsorption on the catalyst surfaces. The $-NH_2$ groups on the surface of IRMOF-3 show an energetically preferable interaction with the $-NO_2$ groups of **A**, 7.83 kcal mol^{-1} lower than that of the C=O groups of **A** (Figure S16). Accordingly, when the core–shell Pd@IRMOF-3 hybrids are used as the catalysts, **A** prefers entering into the nanostructures with the $-NO_2$ group ahead. After entering, the pore dimension of the core–shell nanostructures becomes another important factor in determining the selectivity of **C**. To testify the pore effect, both a shorter molecule, 4-nitro-1-butene (0.87 × 0.53 nm) as an alternative for **B**, and a longer substrate, 4-nitrocinnamaldehyde (1.28 × 0.72 nm) as a replacement for **A**, are utilized in the cascade reaction under the same conditions (Figures S15b,c, S17). When the shorter is used, the selectivity of 4-amino-1-butane and 4-nitro-1-butane is 56% and 44%, respectively; whereas the selectivity reaches 96% for 2-(3-(4-aminophenyl)allylidene)malononitrile when the longer is adopted (Figures S18, S19 and Table S2). It is noticed that the length of the shorter 4-nitro-1-butene is smaller than the average pore size of 1.03 nm, and thus it could freely rotate and associate with amino group on the cavity walls, leading to decrease in the yield of 4-amino-1-butane. On the contrary, the longer 4-nitrocinnamaldehyde must keep the constant direction with the $-NO_2$ group ahead inside the IRMOF-3 channels, because its chain length is considerably larger than the average pore size of 1.03 nm, giving rise to the enhanced selectivity. In addition, the cracks or grain boundaries may be present in the IRMOF-3 shell, which offer the possibility of diffusion of the substrate **A** to the Pd cores without passing through the IRMOF-3 channels. To exclude this effect, a larger substrate, 7-nitroindole-3-carboxaldehyde (1.05 × 0.92 nm) is also used to perform the cascade reaction (Figure S15d). It is clear that only Knoevengel condensation is carried out completely, while the subsequent hydrogenation reaction does not happen (Figure S20 and Table S2). This result suggests that **A** should preferably migrate through the pore channels of IRMOF-3 rather than the cracks or grain boundaries and further discloses that the improved selectivity of **C** over **D** should originate from the unique core–shell nanostructures. Therefore, construction of the core–shell Pd@IRMOF-3 nanocomposites not only realizes catalytic conversion in the cascade reactions but also improves the yield of the target products compared with the supported catalysts.

Another key parameter to evaluate the catalytic performance is stability of the catalyst. Figure S21 demonstrates the conversion of **A** and the selectivity of intermediate product **B** to **C** over five successive cycles for both Pd@IRMOF-3 and Pd/IRMOF-3. Thanks to the high stability of the amino groups in IRMOF-3, both Pd@IRMOF-3 and Pd/IRMOF-3 can catalyze the full conversion of **A** during all repeated cycles (Figure S22). Remarkably, the core–shell Pd@IRMOF-3 hybrids can catalyze hydrogenation of **B** to **C** with the same selectivity of ~86% and exhibit an excellent stability over five successive cycles (Figure S23a–d). On the contrary, the deactivation occurs over the

dx.doi.org/10.1021/ja411468e | J. Am. Chem. Soc. 2014, 136, 1738–1741

supported Pd/IRMOF-3, and the selectivity of **B** to **C** is gradually decreased from 71% to 44% due to the migration and sintering of Pd NPs during the repeated cycles (Figure S23e–h). Evidently, the core–shell Pd@IRMOF-3 nanocomposites are highly stable against the migration and sintering of Pd NPs and exhibit excellent activity, selectivity, and stability for the cascade reactions with respect to the conventional Pd/IRMOF-3.

In summary, the multifunctional core–shell Pd@IRMOF-3 nanocatalysts, for which a Pd NP core is coated with uniform amino-functionalized IRMOF-3 shell, can be readily prepared by a facile mixed solvent method. Impressively, the core–shell nanocomposites could effectively and efficiently realize the cascade catalysis of Knoevenagel condensation of **A** and malononitrile to form **B** via the alkaline IRMOF-3 shells coupled with subsequent hydrogenation of the intermediate product **B** using the Pd NP cores. Compared with the conventional supported Pd/IRMOF-3 catalysts, the core–shell Pd@IRMOF-3 nanostructures show preferential selective hydrogenation of $-NO_2$ groups of the intermediate products **B**, thus considerably improving the yield of the target products **C**. The corresponding DFT calculations and experimental evidence disclose that the characteristic core–shell structures are the origin to improve the selectivity of the cascade reactions. Furthermore, the core–shell Pd@IRMOF-3 hybrids are easily recoverable and can be recycled without loss of catalytic activity in the repetitive reuse cycles. Such a rational design on the nanocomposites of the noble metal NPs and MOFs will open up opportunities for design and fabrication of high-performance multifunctional catalysts.

■ ASSOCIATED CONTENT

Ⓢ Supporting Information

Experimental and theoretical calculation details and additional figures. This material is available free of charge via the Internet at http://pubs.acs.org.

■ AUTHOR INFORMATION

Corresponding Authors

zytang@nanoctr.cn
liguodong@nanoctr.cn

Notes

The authors declare no competing financial interest.

■ ACKNOWLEDGMENTS

This work was supported financially by National Research Fund for Fundamental Key Project (2014CB931801, Z.Y.T.; 2012CB933001, K.D.), National Natural Science Foundation for Distinguished Youth Scholars of China (21025310, Z.Y.T.), National Natural Science Foundation of China (91027011, Z.Y.T.; 21303029, G.D.L.; 20933008, K.D.).

■ REFERENCES

(1) (a) Ferey, G. *Chem. Soc. Rev.* **2008**, *37*, 191. (b) Long, J. R.; Yaghi, O. M. *Chem. Soc. Rev.* **2009**, *38*, 1213. (c) Cook, T. R.; Zheng, Y.-R.; Stang, P. J. *Chem. Rev.* **2013**, *113*, 734.

(2) (a) Farrusseng, D.; Aguado, S.; Pinel, C. *Angew. Chem., Int. Ed.* **2009**, *48*, 7502. (b) Lee, J.; Farha, O. K.; Roberts, J.; Scheidt, K. A.; Nguyen, S. T.; Hupp, J. T. *Chem. Soc. Rev.* **2009**, *38*, 1450. (c) Corma, A.; García, H.; Llabrés i Xamena, F. X. *Chem. Rev.* **2010**, *110*, 4606.

(3) (a) Ma, L.; Abney, C.; Lin, W. *Chem. Soc. Rev.* **2009**, *38*, 1248. (b) Liu, Y.; Xuan, W.; Cui, Y. *Adv. Mater.* **2010**, *22*, 4112. (c) Yoon, M.; Srirambalaji, R.; Kim, K. *Chem. Rev.* **2012**, *112*, 1196. (d) Zhang, L.; Wu, H. B.; Madhavi, S.; Hng, H. H.; Lou, X. W. *J. Am. Chem. Soc.* **2012**, *134*, 17388.

(4) (a) Huang, Y.; Xu, S.; Lin, V. S. Y. *Angew. Chem., Int. Ed.* **2011**, *50*, 661. (b) Shiju, N. R.; Alberts, A. H.; Khalid, S.; Brown, D. R.; Rothenberg, G. *Angew. Chem., Int. Ed.* **2011**, *50*, 9615. (c) Yamada, Y.; Tsung, C.-K.; Huang, W.; Huo, Z.; Habas, S. E.; Soejima, T.; Aliaga, C. E.; Somorjai, G. A.; Yang, P. *Nat. Chem.* **2011**, *3*, 372. (d) Fang, X.; Liu, Z.; Hsieh, M.-F.; Chen, M.; Liu, P.; Chen, C.; Zheng, N. *ACS Nano* **2012**, *6*, 4434. (e) Longstreet, A. R.; McQuade, D. T. *Acc. Chem. Res.* **2012**, *46*, 327. (f) Yang, Y.; Liu, X.; Li, X.; Zhao, J.; Bai, S.; Liu, J.; Yang, Q. *Angew. Chem., Int. Ed.* **2012**, *51*, 9164.

(5) (a) El-Shall, M. S.; Abdelsayed, V.; Khder, A. E. R. S.; Hassan, H. M. A.; El-Kaderi, H. M.; Reich, T. E. *J. Mater. Chem.* **2009**, *19*, 7625. (b) Liu, H.; Liu, Y.; Li, Y.; Tang, Z.; Jiang, H. *J. Phys. Chem. C* **2010**, *114*, 13362. (c) Zlotea, C.; Campesi, R.; Cuevas, F.; Leroy, E.; Dibandjo, P.; Volkringer, C.; Loiseau, T.; Férey, G. R.; Latroche, M. *J. Am. Chem. Soc.* **2010**, *132*, 2991. (d) Jiang, H.-L.; Akita, T.; Ishida, T.; Haruta, M.; Xu, Q. *J. Am. Chem. Soc.* **2011**, *133*, 1304. (e) Aijaz, A.; Karkamkar, A.; Choi, Y. J.; Tsumori, N.; Rönnebro, E.; Autrey, T.; Shioyama, H.; Xu, Q. *J. Am. Chem. Soc.* **2012**, *134*, 13926. (f) Wang, C.; deKrafft, K. E.; Lin, W. *J. Am. Chem. Soc.* **2012**, *134*, 7211.

(6) (a) Kuo, C.-H.; Tang, Y.; Chou, L.-Y.; Sneed, B. T.; Brodsky, C. N.; Zhao, Z.; Tsung, C.-K. *J. Am. Chem. Soc.* **2012**, *134*, 14345. (b) Lu, G.; Li, S.; Guo, Z.; Farha, O. K.; Hauser, B. G.; Qi, X.; Wang, Y.; Wang, X.; Han, S.; Liu, X.; DuChene, J. S.; Zhang, H.; Zhang, Q.; Chen, X.; Ma, J.; Loo, S. C. J.; Wei, W. D.; Yang, Y.; Hupp, J. T.; Huo, F. *Nat. Chem.* **2012**, *4*, 310. (c) Mondloch, J. E.; Bury, W.; Fairen-Jimenez, D.; Kwon, S.; DeMarco, E. J.; Weston, M. H.; Sarjeant, A. A.; Nguyen, S. T.; Stair, P. C.; Snurr, R. Q.; Farha, O. K.; Hupp, J. T. *J. Am. Chem. Soc.* **2013**, *135*, 10294.

(7) (a) Liang, X.; Li, J.; Joo, J. B.; Gutiérrez, A.; Tillekaratne, A.; Lee, I.; Yin, Y.; Zaera, F. *Angew. Chem., Int. Ed.* **2012**, *51*, 8034. (b) Zhang, Q.; Zhang, T.; Ge, J.; Yin, Y. *Nano Lett.* **2008**, *8*, 2867. (c) Herves, P.; Perez-Lorenzo, M.; Liz-Marzan, L. M.; Dzubiella, J.; Lu, Y.; Ballauff, M. *Chem. Soc. Rev.* **2012**, *41*, 5577. (d) Khaletskaya, K.; Reboul, J.; Meilikhov, M.; Nakahama, M.; Diring, S.; Tsujimoto, M.; Isoda, S.; Kim, F.; Kamei, K.; Fischer, R. A.; Kitagawa, S.; Furukawa, S. *J. Am. Chem. Soc.* **2013**, *135*, 10998.

(8) Wang, F.; Li, C.; Sun, L.-D.; Xu, C.-H.; Wang, J.; Yu, J. C.; Yan, C.-H. *Angew. Chem., Int. Ed.* **2012**, *51*, 4872.

(9) Eddaoudi, M.; Kim, J.; Rosi, N.; Vodak, D.; Wachter, J.; O'Keeffe, M.; Yaghi, O. M. *Science* **2002**, *295*, 469.

(10) (a) Hasegawa, S.; Horike, S.; Matsuda, R.; Furukawa, S.; Mochizuki, K.; Kinoshita, Y.; Kitagawa, S. *J. Am. Chem. Soc.* **2007**, *129*, 2607. (b) Gascon, J.; Aktay, U.; Hernandez-Alonso, M. D.; van Klink, G. P. M.; Kapteijn, F. *J. Catal.* **2009**, *261*, 75.

(11) (a) Tirelli, N.; Altomare, A.; Solaro, R.; Ciardelli, F.; Meier, U.; Bosshard, C.; Günter, P. *J. Prakt. Chem.* **1998**, *340*, 122. (b) Sato, N.; Yuki, Y.; Shinohara, H.; Takeji, Y.; Ito, K.; Michikami, D.; Hino, K.; Yamazaki, H. Patent US 2012/0022077.

(12) (a) Zhang, N.; Fu, X.; Xu, Y.-J. *J. Mater. Chem.* **2011**, *21*, 8152. (b) He, L.; Liu, Y.; Liu, J.; Xiong, Y.; Zheng, J.; Liu, Y.; Tang, Z. *Angew. Chem., Int. Ed.* **2013**, *52*, 3741.

(13) Surble, S.; Millange, F.; Serre, C.; Ferey, G.; Walton, R. I. *Chem. Commun.* **2006**, *14*, 1518.

(14) (a) Guerrero-Martínez, A.; Pérez-Juste, J.; Liz-Marzán, L. M. *Adv. Mater.* **2010**, *22*, 1182. (b) Yu, L.; Zhang, G.; Yuan, C.; Lou, X. W. *Chem. Commun.* **2013**, *49*, 137.

(15) Nguyen, L. T. L.; Le, K. K. A.; Truong, H. X.; Phan, N. T. S. *Catal. Sci. Technol.* **2012**, *2*, 521.

(16) (a) Liu, J.; Qiao, S. Z.; Chen, J. S.; Lou, X. W.; Xing, X.; Lu, G. Q. *Chem. Commun.* **2011**, *47*, 12578. (b) Zhang, C.; Wu, H. B.; Yuan, C.; Guo, Z.; Lou, X. W. *Angew. Chem., Int. Ed.* **2012**, *51*, 9592. (c) Zhang, Q.; Lee, I.; Joo, J. B.; Zaera, F.; Yin, Y. *Acc. Chem. Res.* **2013**, *46*, 1816. (d) Liu, J.; Yang, H. Q.; Kleitz, F.; Chen, Z. G.; Yang, T.; Strounina, E.; Lu, G. Q.; Qiao, S. Z. *Adv. Funct. Mater.* **2012**, *22*, 591.